Decay branching ratios of excited ^{24}Mg

J. M. Munson, E. B. Norman, J. T. Burke, R. J. Casperson, L. W. Phair, E. McCleskey, M. McCleskey, D. Lee, R. O. Hughes, S. Ota, A. Czeszumska, P. A. Chodash, A. J. Saastamoinen, R. A. E. Austin, A. E. Spiridon, M. Dag, R. Chyzh, M. S. Basunia, J. J. Ressler, and T. J. Ross

Phys. Rev. C **95**, 015805 — Published 19 January 2017

DOI: 10.1103/PhysRevC.95.015805

Decay branching ratios of excited ^{24}Mg

J. M. Munson,[1] E. B. Norman,[1] J. T. Burke,[2] R. J. Casperson,[2] L. W. Phair,[3] E. McCleskey,[4] M. McCleskey, D. Lee,[5] R. O. Hughes,[2] S. Ota,[2] A. Czeszumska,[1,2] P. A. Chodash,[2] A. J. Saastamoinen,[4] R. A. E. Austin,[6] A. E. Spiridon,[4] M. Dag,[4] R. Chyzh,[4] M. S. Basunia,[3] J. J. Ressler,[2] and T. J. Ross[7]

[1]*Department of Nuclear Engineering, University of California, Berkeley, CA 94720 USA*
[2]*Nuclear and Chemical Sciences Division, Lawrence Livermore National Laboratory, Livermore, CA 94550 USA*
[3]*Nuclear Science Division, Lawrence Berkeley National Laboratory, Berkeley, CA 94720 USA*
[4]*Cyclotron Institute, Texas A&M University, College Station, TX 77843 USA*
[5]*Engineering Division, Lawrence Berkeley National Laboratory, Berkeley, CA 94720 USA*
[6]*St. Mary's College, Halifax, Nova Scotia, Canada*
[7]*Department of Physics, University of Richmond, Richmond, VA 32173 USA*

(Dated: December 19, 2016)

The nuclear reactions ^{12}C(^{12}C, α)^{20}Ne, ^{12}C(^{12}C, p)^{23}Na, and ^{12}C(^{12}C, n)^{23}Mg are the primary reactions in carbon burning, which occurs as part of several stellar processes. The Gamow window, which describes the energy range where most of these reactions take place, is typically around 1.5 MeV in the center of mass frame. Direct measurements of the cross sections at this energy are difficult due to the large Coulomb barrier present between the carbon nuclei, however a successful surrogate measurement can provide the branching ratios between these reactions while avoiding the $^{12}\mathrm{C} + ^{12}\mathrm{C}$ Coulomb barrier. An experiment was performed using inelastic scattering of 40 MeV α particles on ^{24}Mg as a possible surrogate for the $^{12}\mathrm{C} + ^{12}\mathrm{C}$ compound nucleus.

PACS numbers: 24.87.+y, 26.20.Np, 26.30.-k, 27.30.+t

I. INTRODUCTION

During carbon burning in stars, carbon undergoes the reactions $^{12}\mathrm{C} + ^{12}\mathrm{C} \rightarrow ^{20}\mathrm{Ne} + \alpha$, $^{12}\mathrm{C} + ^{12}\mathrm{C} \rightarrow ^{23}\mathrm{Na} + \mathrm{p}$, and $^{12}\mathrm{C} + ^{12}\mathrm{C} \rightarrow ^{23}\mathrm{Mg} + \mathrm{n}$. These reactions proceed through a short lived compound nucleus of excited ^{24}Mg. At a typical carbon burning temperature of 5×10^8 K the reactions take place at a center of mass energy of 1 to 2 MeV, corresponding to an excitation energy in the ^{24}Mg nucleus of 15 to 16 MeV [1]. In the present work, the decay branching ratios of ^{24}Mg excited to energies up to 27 MeV were studied[2]. The ^{24}Mg was excited using the inelastic scattering of 40 MeV α particles. In addition to providing data on inelastic scattering itself, this measurement was selected to gain knowledge about stellar carbon burning.

In the Bohr hypothesis the cross section for each reaction is the product of the formation cross section for the compound nucleus and the branching ratio for the compound nucleus to decay by the corresponding exit channel[3]. Since the ^{24}Mg compound nucleus is formed with a high excitation energy, many overlapping states in the compound nucleus can contribute. The formation cross section for a given excited energy is the sum of the formation cross sections for each underlying state. The branching ratio is a weighted average of the branching ratios of the populated nuclear states. In particular, there will be a distribution of excited states in the excited nucleus with regards to energy, spin, and parity.

The surrogate method is an approach to studying cross sections that makes use of the compound nucleus assumption[4, 5]. Since the branching ratios are a function of the compound nucleus, the same compound nucleus produced by a different formation reaction will still have similar branching ratios, assuming that the distribution of the excited states is the same. However, since different formation reactions may produce compound nuclei with different spin and parity distributions, assumptions must often be made as to how the surrogate compound nucleus compares to the desired compound nucleus. For this reason it is desirable to compare surrogate results to direct results when possible. Direct measurements for carbon burning have been made down to 2.1 MeV [6–12] This is higher than the 1 to 2 MeV energy window of primary interest to stellar carbon burning. This work uses the surrogate approach to measure the decay branching ratios of the ^{24}Mg nucleus excited to energies corresponding to this energy window in carbon burning.

II. SURROGATE METHOD

The surrogate method is an approach to indirectly measuring compound reaction cross sections by using an alternate reaction to produce a nucleus in a state corresponding to that of the compound nucleus of the reaction of interest [4]. The surrogate method has been used to measure fission and other cross sections for a number of heavy nuclei by the STARS/LiBerACE [4, 13] and successor STARLiTe and STARLiTeR groups. For a number of these experiments, direct (n, f) measurements were impractical due to the short half life of the target nuclei, requiring other reactions on neighboring nuclei ("surrogate reactions") to be measured in order to infer the desired (n, f) cross section.

The key items to match are the number of protons and neutrons, the excitation energy, and spin and parity distributions. In the case of $^{12}\mathrm{C} + ^{12}\mathrm{C}$ reactions, the

compound nucleus is ^{24}Mg. The Q value going to the compound nucleus is 13.934 MeV. As the stellar reactions of interest occur at energies around 1.5 MeV, a typical excitation energy of interest in the compound nucleus is around 15.5 MeV. Direct measurements of the reaction have been made in the range of 2.1 to 6 MeV, corresponding to excitation energies of 16.1 to 20 MeV in ^{24}Mg. A nuclear reaction that produces ^{24}Mg in a range of excitation energies between 14 and 20 MeV is desired.

The difference in the reaction rates as a result of the possible spin differences in the $^{12}C + ^{12}C$ compound nucleus and the surrogate reaction can be neglected if certain criteria are met [14, 15]. A primary condition is that the excitation energy must be sufficiently high that the possible branches are dominated by level density integrals rather than individual states [16]. This independence of the branching ratios from spin and parity is called the Weisskopf-Ewing approximation [17]. For carbon burning reactions this is met for the compound nucleus but not for the daughter nuclei, therefore matching the spin distribution for the excited nucleus to the extent possible is still important to minimize the change in branching ratios that may occur due to differences in spin distributions.

The approach that was selected is to excite ^{24}Mg using inelastic scattering. Using scattering to excite the nucleus allows for the scattered particle to be used to identify the excitation energy produced in ^{24}Mg. By identifying the excitation of the ^{24}Mg nucleus on a per event basis the correct excitation distribution with respect to energy can be reconstructed for a range of different stellar temperatures.

Lighter ions are preferred for the inelastic excitation for a few reasons. First is that lighter ions will provide a much clearer signature in the ΔE-E silicon detector setup after scattering. Second, protons and α particles will not become excited themselves and further complicate the excitation measurement for the ^{24}Mg nucleus. Finally, lighter ions will transfer less angular momentum during collision. As the beam will have a much higher energy than the kinetic energy of the $^{12}C + ^{12}C$ reaction, it is possible that higher angular momentum states are excited. An α particle beam was ultimately selected since α particles favorably populate the same parity pattern (0+, 2+, etc.) and because the scattered α particles have a convenient stopping range in the silicon detector setup.

III. EXPERIMENTAL SETUP

An experiment was performed which used an α particle beam to inelastically excite ^{24}Mg and identify the resulting decay products using the outgoing α particles and protons as well as the characteristic γ-rays from the resulting ^{20}Ne, ^{23}Na, and ^{23}Mg daughters. The experiment was performed at the K150 cyclotron at the Texas A&M Cyclotron Institute using the STARLiTeR detector array. The STARS target chamber [13] was loaded with two silicon detectors in a ΔE-E arrangement, described in Section III C. The chamber was surrounded by six germanium detectors, described in Section III D. Each germanium detector was housed inside a BGO detector which was used to veto Compton scattering events. The setup is shown in Fig. 1.

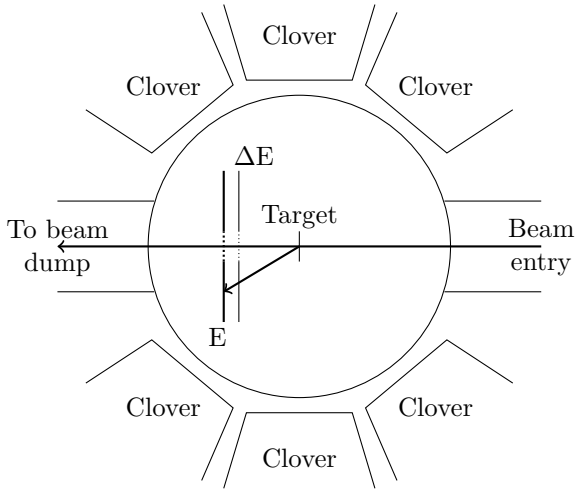

FIG. 1. Experimental setup showing the ΔE and E silicon detectors and target within the STARS chamber and six "Clover" HPGe detectors surrounding the chamber.

A. Targets

The STARS chamber[13] is designed to hold up to eight targets. A knob is located outside the target chamber which can be manually turned in order to select which target is in the path of the beam. The targets used are listed in Table I.

Description	Accumulated charge	Beam time
^{24}Mg Primary (155 μg/cm^2)	620 μC	109 hours
^{24}Mg Backup (262 μg/cm^2)	11.1 μC	138 minutes
Natural Carbon (50 μg/cm^2)	29 μC	315 minutes
Mylar (2 mil)	132 nC	86 minutes
^{208}Pb	630 nC	64 minutes

TABLE I. Targets used for each run and the approximate amount of beam each target received.

The primary target was a thin, self supporting ^{24}Mg target. The magnesium used for the enriched targets was obtained from Oak Ridge National Laboratory and is $99.9\% \pm 0.02\%$ ^{24}Mg. Impurities in the feed material as stated by ORNL include 300 ppm Na and 700 ppm Mo. Oxygen and carbon are both apparent in the data collected during the run and could have been introduced during the production, handling, or use of the

targets. The targets were made using evaporation deposition of magnesium onto glass slides coated and buffed with Liquinox soap. The foils were then removed by sliding a razor along the glass, creating a rolled tube of magnesium. This rolled tube was unrolled by placing it on a piece of plastic which was then given a small electrostatic charge using a cotton swab. Once the foil was unrolled, a glue coated target frame was placed directly on top of the foil and slowly lifted. The main target was the thinnest target produced using this method. The target thickness was measured in two ways. The first was using a second glass slide coated at the same time as the main target. This slide was measured to have 174 μg/cm^2 at the center using a profilometer. The thickness was also measured using an α particle source and a silicon detector, and by relating the energy lost by the α particle to the thickness of the target. This measurement gave a thickness of 155 ± 10 μg/cm^2. Since this experiment was designed to measure ratios, the primary importance of the thickness measurement is to properly account for the energy lost by the particle within the target. Using a thin target minimizes this energy loss and the associated energy uncertainty.

Natural carbon and Mylar targets were used to subtract the effects of the carbon and oxygen contamination on the magnesium target. Data from a ^{208}Pb target was used in conjunction with the other lower Z targets to measure the beam energy, beam position, and target distance following the experiment.

B. Beam

An α particle beam with a nominal energy of 40 MeV was delivered by the Texas A&M Cyclotron Institute K150 cyclotron. During analysis, the beam energy was considered a free parameter which was fitted using the energy of scattered beam at different angles for the various target masses (^{12}C, ^{24}Mg, and ^{208}Pb). The value adopted from this fitting was 39.58 MeV at the beginning of the run and 39.33 MeV at the end of the run. The change in the fitted value occurred over a period of about 24 hours during the middle of the week long run. Fits within each stable period had a scatter of approximately 0.07 MeV.

The beam current was held in the range of 0.5 to 2 nA when the primary ^{24}Mg target was in place. Event pileup for the silicon detectors was the limiting factor, so the beam current was adjusted for the primary target based on the silicon detector trigger rate. The beam current for other targets (carbon, Mylar, etc.) was adjusted such that the master trigger rate was similar to that of the main target, typically around 7 to 10 kHz.

C. Silicon Detectors

Micron Semiconductor "S2" type silicon detectors were used to detect and measure the outgoing charged particles. These detectors are annular, with a hole in the center for the nonscattered beam to pass through. The silicon is divided into 48 rings and 16 sectors which allows for the polar angle from the beam and the azimuthal angle around the beam to be recorded. This segmentation also allows for a single detector to record multiple particle hits. The inner ring is located at a radius of 11 mm and the outer ring at 35 mm, making each ring 0.5 mm wide. Two such detectors were arranged in a ΔE-E configuration. The ΔE detector had a thickness of 62 μm and was located 2 cm downstream from the target. The E detector had a thickness of 1 mm and was placed 1 cm behind the ΔE detector. Adjacent rings and adjacent sectors of the E detector were paired and connected to the same preamp channel. This reduced the total number of channels read out and gave the E detector 24 effective rings and 8 effective sectors. The 62 μm ΔE detector allowed protons down to approximately 3 MeV to pass through to the E detector and be differentiated from α particles based on energy loss in the ΔE detector. The scattered α particles which left the target ^{24}Mg with an excitation of less than 27 MeV also had sufficient energy to pass through the ΔE detector and be identified based on energy loss in the ΔE detector. The silicon detectors covered an angular range of 31 degrees to 61 degrees for particles stopping in the ΔE detector, and 31 degrees to 50 degrees for particles passing through the ΔE detector and stopping in the E detector.

D. Germanium Detectors

Six segmented Canberra "clover" HPGe detectors were placed around the target chamber for the detection of γ-rays emitted from the reaction. Each clover detector was positioned inside a BGO detector which was used to veto signals resulting from Compton scattered γ-rays. This veto reduces the Compton continuum present in the γ-ray energy spectrum while maintaining the full energy events.

Since the γ-rays of interest are emitted from nuclei that may have a recoil energy of several MeV it is necessary to apply a Doppler correction to the detected γ-ray energy to determine the γ-ray energy in the rest frame of the nucleus. The Doppler correction was calculated using the velocity of the recoiling ^{24}Mg nucleus as calculated from the scattered α particle. While this velocity is not exactly equal to the velocity of the ^{20}Ne or ^{23}Na product nuclei, it is close enough to provide adequate Doppler correction and can be done without prior knowledge of which final product is produced or what energy and angle the emitted α particle or proton has.

Most lines were well separated when they had sufficient counts to be visible. An important exception is the 1634

keV line from the first excited state of ^{20}Ne and the 1636 keV line from the second excited state of ^{23}Na decaying to the first excited state. It is unlikely that these lines could be resolved even without the additional complication of the Doppler shift. A separation of the 1634 keV γ-ray was made using the ejected particle data as detailed in Section IV D.

The effect of the lab frame dipole component of the γ-ray angular distribution on the detection efficiency is to a large degree canceled out due to the symmetry of the upstream and downstream HPGe detectors. Since two of the four germanium crystals in one downstream detector and one crystal in one upstream detector were not used the cancellation is imperfect. The effect of the quadrapole component does not cancel out. The dipole and quadrapole components in the lab frame were estimated for each γ-ray by comparing the count rates at the three angles. Corrections to the γ-ray detection efficiency are shown in Table II. Higher order angular components are not included in the correction.

γ-ray	Isotope	Correction factor
1369	^{24}Mg	0.948 ± 0.002
4238	^{24}Mg	1.072 ± 0.015
1634	^{20}Ne or ^{23}Na	1.027 ± 0.002
2613	^{20}Ne	1.036 ± 0.004
3333	^{20}Ne	0.985 ± 0.011
440	^{23}Na	1.024 ± 0.001
2076	^{23}Na	1.085 ± 0.024
2390	^{23}Na	1.042 ± 0.035
627	^{23}Na	0.990 ± 0.003
451	^{23}Mg	1.002 ± 0.003

TABLE II. γ-ray detection efficiency correction due to the γ-ray angular distribution. A 2.5% systematic uncertainty for the correction factor was assumed in addition to the statistical uncertainty listed here.

IV. ANALYSIS AND RESULTS

A. Particle Identification

The identification of the scattered α particles and ejected protons with energies above 3 MeV was based on the energy loss in the ΔE detector as compared to the total particle energy found by adding the energy loss in the ΔE detector and the E detector. Some deuterons and tritons were also identified using this method and these events were excluded from the analysis. Figure 2 shows the measured energy loss in the ΔE detector divided by the path length of the particle in the ΔE detector for particles of different total energy. Dividing by the path length accounts for the greater energy a particle at a high angle would leave in the ΔE detector due to longer path through the detector.

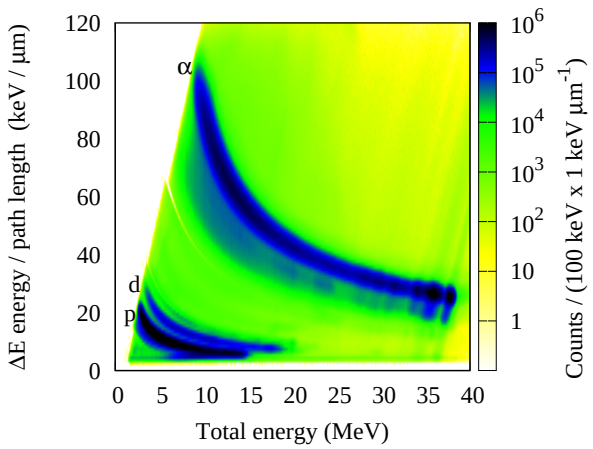

FIG. 2. (Color online) ΔE Energy Loss Rate vs Particle Energy for particle identification. Here the energy deposited in the ΔE silicon detector is divided by the path length of the particle through the detector. Since the ΔE is a thin detector, this places a particular particle on the same curve for all measured angles. The labels p and d refer to protons and deuterons. A faint band from tritons is present just above the band for deuterons. The hook in the proton band at 15 MeV is from higher energy protons passing through both the ΔE and E detectors, thus not depositing their full energy.

B. Magnesium Excitation

The excitation of the ^{24}Mg nucleus was determined from the scattered α particle energy and angle. The distribution of excited states detected is shown in Fig. 3. Scattering events which did not lead to the detection of an α particle in the silicon detectors are not included.

Carbon and oxygen were found to be present on the magnesium target. To subtract the contribution of the carbon and the oxygen a natural carbon target and a Mylar target were each used in place of the magnesium target periodically throughout the experiment. The ratios for subtracting the carbon and Mylar target spectra from the magnesium spectra were determined by matching the elastic peaks for carbon and oxygen in the excitation spectrum found from the scattered α particles. Due to the different recoil kinetic energies, the energy of the elastically scattered α particles has a different dependence on angle for each target mass. This dependence allowed the elastic peaks to be identified despite the fact that at some angles the elastic peak for the lighter carbon and oxygen targets had the same α particle energy as α particles which left ^{24}Mg in its first excited state.

C. Particle-Particle Coincidence

One method of identifying the outgoing branch is by looking for a coincidence of the scattered α particle and the α particle or proton emitted from the excited ^{24}Mg nucleus. The energy and angle of the scattered α parti-

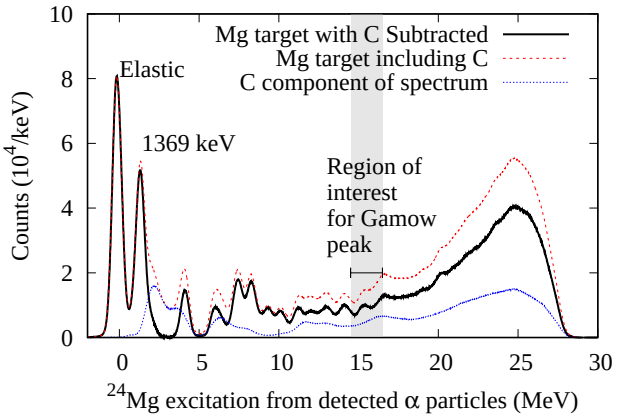

FIG. 3. (Color online) The spectrum of excitation in ^{24}Mg corresponding to detected α particles, integrated over all measured scattering angles. The contribution from ^{12}C present in the target is also shown.

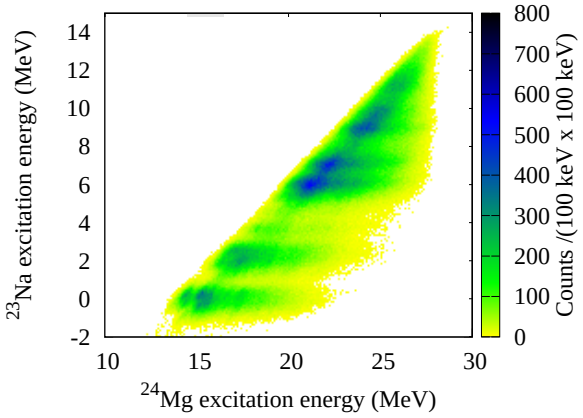

FIG. 4. (Color online) The excitation of the ^{23}Na daughter as a function of the ^{24}Mg excitation found with the scattered α particle. A proton ΔE-E particle identification was required for the ejected proton.

cle determines the excitation produced in ^{24}Mg and with this knowledge the energy and angle of the emitted particle determines the excitation of the ^{20}Ne or ^{23}Na product nucleus. At proton energies above 3 MeV when the proton can be identified using the ΔE-E method the product nucleus is known and only the excitation of the product ^{23}Na needs to be determined. This is shown in Fig. 4. At lower energies the ejected particle cannot be identified as a proton or α particle using the ΔE-E method. Instead the excitation of the daughter nuclide is calculated based first on the kinematics for an ejected proton and plotted and then again based on the kinematics for an ejected α particle. This results in Fig. 5 and Fig. 6. Events will fall on horizontal bands corresponding to the energy levels of the daughter nuclide on the plot corresponding to the ejected particle type, and will fall on offset

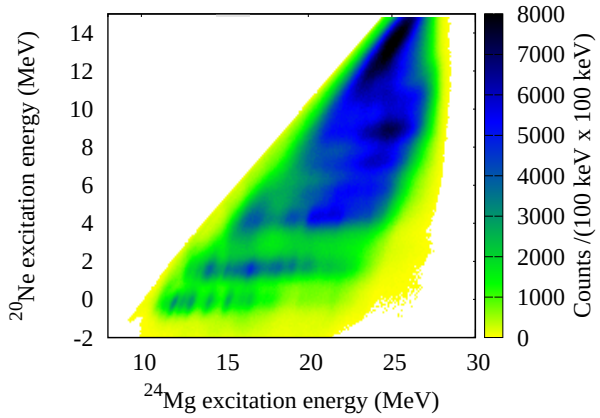

FIG. 5. (Color online) The excitation of the ^{20}Ne daughter as a function of the ^{24}Mg excitation found with the scattered α particle, assuming the ejected particle is an α particle. States in ^{20}Ne can be seen as horizontal bands. Events producing ^{20}Ne in the ground and first excited states were identified in this way.

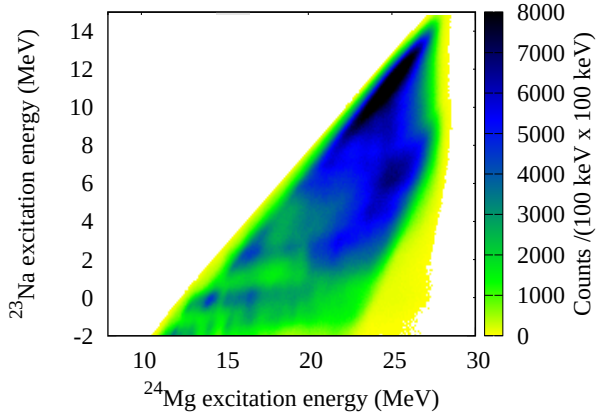

FIG. 6. (Color online) The excitation of the ^{23}Na daughter as a function of the ^{24}Mg excitation found with the scattered α particle. No ΔE-E particle ID was used for the ejected proton. This plot was only used for the range of ^{24}Mg excitation that would lead to a proton with too little energy to pass through the ΔE detector. The α channels leading to ^{20}Ne are visible as slightly sloped horizontal bands.

and sloped bands on the plot corresponding to incorrect particle type. In practice the branches to the ground and first excited states of ^{20}Ne as well as the sum of the branches to the ground and first excited states of ^{23}Na could be measured using this method. The ground and first excited states of ^{23}Na could not be individually resolved using this method alone. Requiring an additional coincidence with the 440 keV γ-ray emitted from the first excited state of ^{23}Na allowed the contribution of each the ground state and first excited state to be separated.

For the ^{20}Ne branch, the higher energy α particle was

treated as the scattered particle. For events corresponding to the Gamow window reversing the α particle assignments would imply a high excitation in ^{24}Mg (around 28 MeV depending on scattering angle) and a correspondingly high emitted α particle energy (around 15 MeV in the recoil frame for populating the ground state of ^{20}Ne), which makes this assignment unlikely. This argument does break down for higher ^{24}Mg excitation energies as the scattered α particle and the ejected α particle energies approach each other. In this case the excitation bin found assuming the higher energy α particle is the scattered particle can include additional counts from the (generally higher) excitation bin that would be found using the lower energy α particle. Since the scattered particle distribution is more forward directed than the ejected particle distribution (which is assumed here to be isotropic in the recoil frame of reference), incorrect α particle assignments will appear more strongly in the branching measurements than in the measured excitation distribution. As a result, an indicator of incorrect assignments is a branching ratio sum that is greater than one. Fig. 3 shows possible evidence of this starting at an ^{24}Mg excitation of 23 MeV, much higher than the excitation energy range corresponding to the Gamow window.

D. Particle-γ Coincidence

For many of the excited states in the product nuclei, requiring a coincidence with a characteristic γ-ray allows a much cleaner identification of the outgoing channel. For the second and third excited states of ^{20}Ne, the second, third, and fifth excited states of ^{23}Na, and the first excited state of ^{23}Mg the identification was made using a coincidence between the scattered α particle and a characteristic γ-ray. The 2076 keV (second excited) state of ^{23}Na is also populated through γ-decay from the fifth excited state requiring this state to be determined prior to the second state and its contribution subtracted from the strength of the second state's characteristic γ-ray.

Reactions populating the first excited state of ^{23}Na at 440 keV were identified using a coincidence between the scattered α particle, the ejected proton, and the characteristic 440 keV γ-ray. Several higher excited states of ^{23}Na will populate the 440 keV state after γ-ray emission. Requiring the extra coincidence with the ejected proton specifically identifies reactions populating the first excited state of ^{23}Na by proton emission from excited ^{24}Mg.

Figure 7 shows the γ-ray spectrum in coincidence with a scattered α particle. Figure 8 shows the γ-ray spectrum as a function of the ^{24}Mg excitation calculated from the coincident scattered α particle. Plotting the γ-rays coincident with the ^{24}Mg excitation shows the γ cascades present in ^{24}Mg and the onset of the particle decay channels.

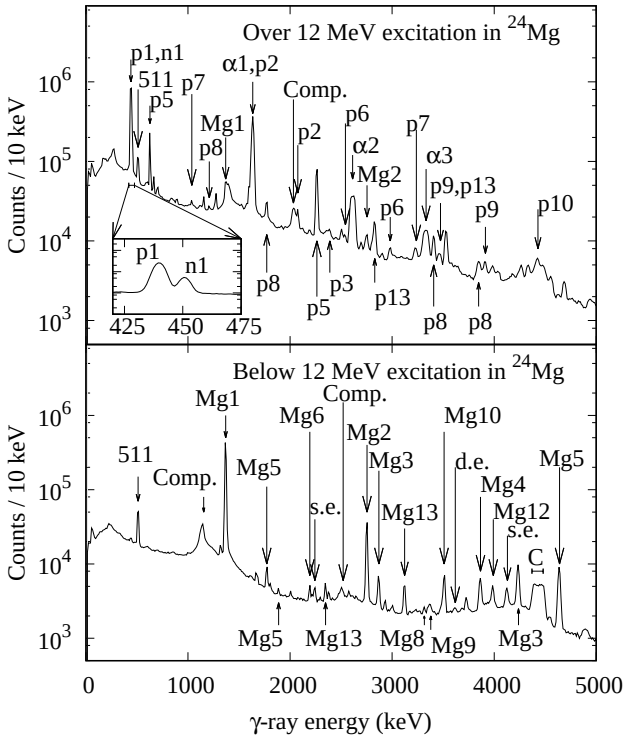

FIG. 7. The γ spectrum produced in coincidence with a scattered α particle. The first spectrum is for events with a ^{24}Mg excitation energy over 12 MeV as indicated by the scattered α particle. The peak at 440 keV has been expanded to show the separation of the 440 keV γ-ray belonging to ^{23}Na and the 451 keV γ-ray belonging to ^{23}Mg. The second spectrum is for events corresponding to a ^{24}Mg excitation energy below 12 MeV. This division gives an approximate split for γ-rays originating from the excited ^{24}Mg nucleus and those for the daughter nuclei ^{20}Ne, ^{23}Na, and ^{23}Mg. The primary contaminants on the target were carbon and oxygen, of which the 4438 keV γ-ray from carbon can be seen. A Doppler correction based on the recoiling ^{24}Mg nucleus has been applied. This is also the approximate correction needed for the daughter nuclei. Due to the difference in mass, the 4438 keV peak from ^{12}C retains some Doppler broadening. Mg, α, p, and n refer to ^{24}Mg, ^{20}Ne, ^{23}Na, and ^{23}Mg, with numbers indicating the excited state.

E. Three Particle Coincidence

Higher excited states of ^{20}Ne decay by α particle emission. The Q-value for ^{20}Ne to emit an α particle is -4.73 MeV[18], and the first excited state to primarily decay by α particle emission is at 5.62 MeV[19]. For this and higher states a coincidence between the scattered α particle and two more particle hits was required. The combined branching ratio for all α particle emitting states of ^{20}Ne was measured in this way. The branching ratios to individual α particle emitting states were not measured.

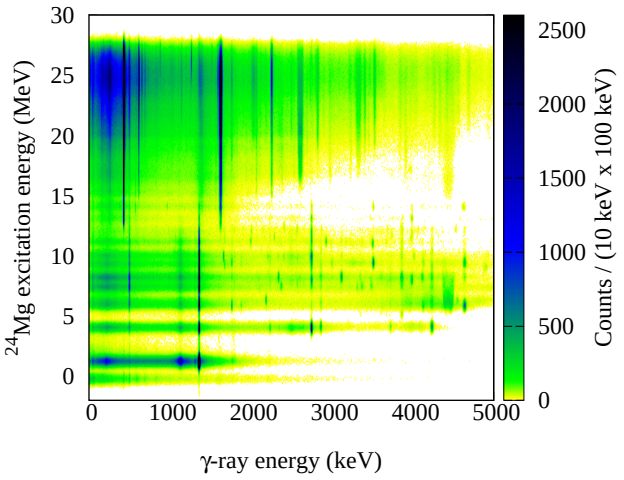

FIG. 8. (Color online) The γ-ray energies vs the excitation of ^{24}Mg as calculated from the coincident scattered α particle. The 1369 keV γ-ray from the first excited state of ^{24}Mg can bee seen strongly at lower excitation energies as it is fed by many of the higher excited states. At around 13 to 14 MeV excitation it can be seen to diminish in favor of the 440 keV γ-ray from ^{23}Na and the 1634 keV γ-ray from ^{20}Ne, showing the opening of the particle decay channels at higher excitation energies. Counts shown in coincidence with elastic scattering (zero on the vertical axis) give a visual estimate of the accidental coincidence γ-ray spectrum. This spectrum would be scaled according to Fig. 3 to estimate the contribution at higher excitation energies.

F. Branching Ratios

The specific methods used to measure each branching ratio are listed in Table III. Each method also required a coincidence with a scattered α particle used to determine the excitation of the ^{24}Mg. The measured branching ratios are shown in Fig. 9 through Fig. 13 along with comparisons to branching ratios for the $^{12}C + ^{12}C$ reaction.

A general trend can be seen in that the branching ratios from the ^{24}Mg excited by inelastic scattering favor higher spin channels as compared to the $^{12}C + ^{12}C$ reaction. The ground state of ^{20}Ne has a spin and parity of 0^+ and the branching ratios for the inelastic scattering case and the carbon burning case compare well. Inelastic scattering measurements for the first (1634 keV) and third (4967 keV) excited states, which have a spin and parity of 2^+ and 2^- respectively, are both higher than for the $^{12}C + ^{12}C$ data, but are within the scatter and error bars. A large deviation is seen for the second excited state (4248 keV) which also has the largest spin of 4^+. In both cases the deviation seems to be shrinking as one moves towards higher excitation energies. The larger branching ratios to higher spin states for inelastically excited ^{24}Mg as compared to $^{12}C + ^{12}C$ causes the total α branching ratio to be larger for the inelastic scattering case for the excitation range of 17 MeV to 19 MeV. It is worth noting however that the contribution of the 4^+ state, which has the largest deviation, is small below an excitation energy of 16 MeV. It is possible then that the branching ratio around the Gamow window of 15 to 16 MeV is again similar to that for inelastic scattering.

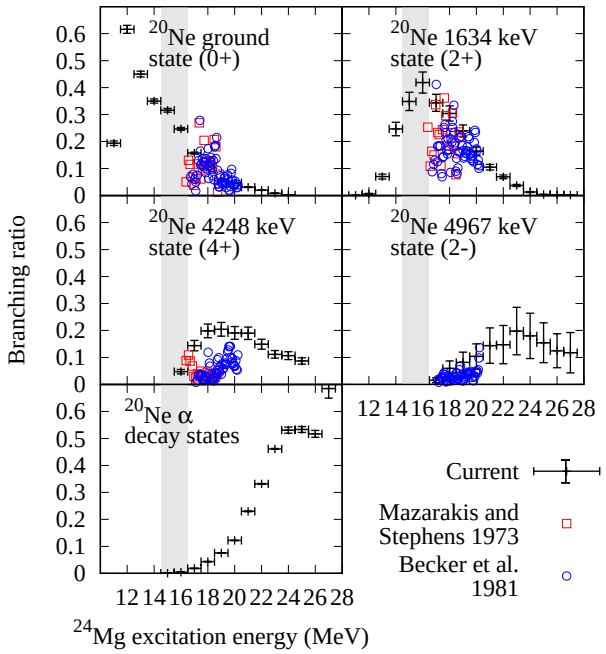

FIG. 9. (Color online) Branching ratios for α particle emitting channels. The bottom plot is the combined branching ratio to excited states of ^{20}Ne that decay by α particle emission, resulting in ^{16}O as the final product.

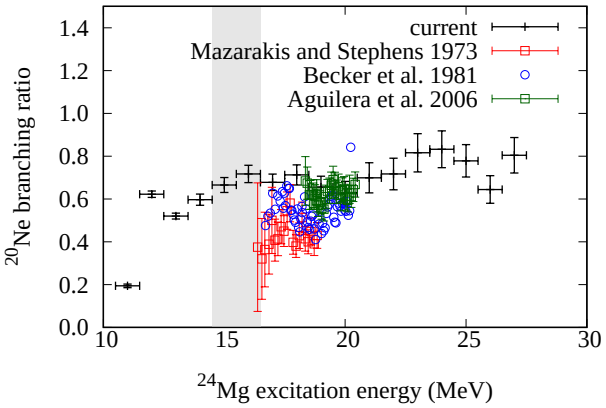

FIG. 10. (Color online) Total α branch (ground plus all excited states of ^{20}Ne). This includes excited states of ^{20}Ne which decay by α particle emission. The reference data is from [7, 9, 11].

The same trend is seen for the branches to states of ^{23}Na. Here the best agreement seems to be with the 2076 keV 7/2+ state, with states of lower spin having branching ratios smaller than that for $^{12}C + ^{12}C$ and the 2704 keV 9/2+ state having a slightly higher branching

Nucleus	Excitation level	Excitation range	Method
^{20}Ne	Ground state	All	Ejected particle, no ΔE-E PID
	1634 keV	All	1634 keV γ-ray in coincidence with ejected particle, no ΔE-E PID
	4248 keV	All	2613 keV γ-ray
	4967 keV	All	3333 keV γ-ray
	α particle emitting states	All	Two ejected particles
^{23}Na	Ground state	Below 15.5 MeV	Ejected particle, no ΔE-E PID, minus 440 keV state contribution
		Above 15.5 MeV	Ejected proton with ΔE-E PID, minus 440 keV state contribution
	440 keV	Below 15.5 MeV	Ejected particle, no ΔE-E PID, in coincidence with a 440 keV γ-ray
		Above 15.5 MeV	Ejected proton, with ΔE-E PID, in coincidence with a 440 keV γ-ray
	2076 keV	All	2076 keV γ-ray minus feeding from 2704 keV level
	2390 keV	All	2390 keV γ-ray
	2704 keV	All	627 keV γ-ray
^{23}Mg	Ground state	n/a	Not measured
	450 keV	All	450 keV γ-ray

TABLE III. Methods used to measure specific exit channels. All channels were measured in coincidence with a scattered α particle.

ratio than for $^{12}C + ^{12}C$ reactions. The fourth excited state of ^{23}Na was not observed, and in the $^{12}C + ^{12}C$ data the fourth and fifth states were not resolved from each other. In the bottom plot of Fig. 11 the sum of the fourth and fifth states is compared to the current measurement for the fifth state alone.

The ground state branch for ^{23}Mg could not be measured in the current setup as the emitted particle is a neutron and not a charged particle, and no neutron detectors were present. The first excited state was measured using the 451 keV γ-ray. No estimate for the ground state contribution was attempted.

G. Normalization

By definition, the sum of the branching ratios of all exit channels is one. Therefore the sum of all the branching ratio measurements should also equal one. In this way summing the measured branching ratios is a check for the measurement. A sum that does not equal one can indicate that the counting efficiency is not known well enough, that some channels are missing, or that the number of counts for some channels includes events not actually belonging to that channel.

In addition to the proton, neutron, and α particle channels the deexcitation of ^{24}Mg by γ-ray emission must be included. This is not a major factor at the excitation energies relevant to carbon burning, but is important at slightly lower excitation energies below the point where particle emission channels open up. Many states in ^{24}Mg which deexcite by γ-decay often do so in a cascade which includes the first excited state at 1369 keV. Because of this, most of the γ branch can be measured by measuring

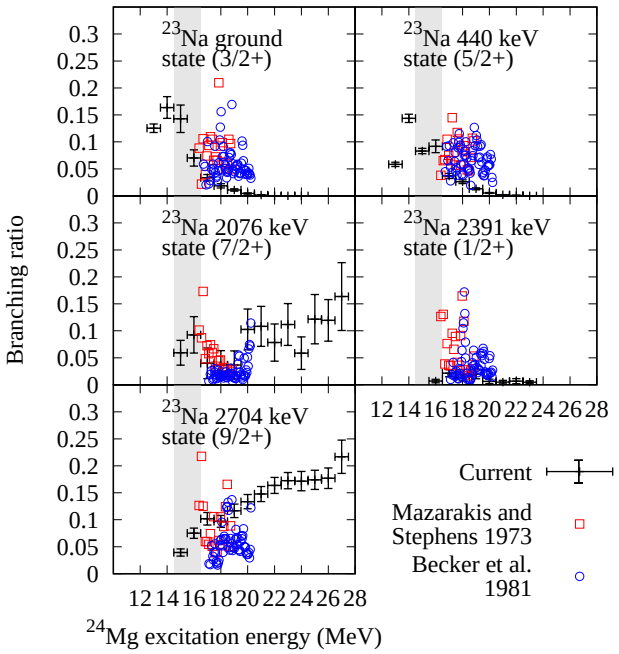

FIG. 11. (Color online) Branching ratios for proton emitting channels. The bottom plot is for the proton branch to the fifth excited state of ^{23}Na. γ-rays from the fourth excited state were not seen. Comparison data for this plot is for the fourth and fifth excited states combined, which were not resolved.

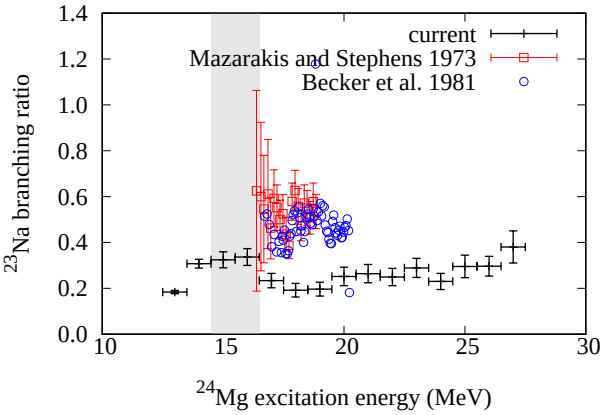

FIG. 12. (Color online) Total proton branching ratio (ground plus all excited states of ^{23}Na)

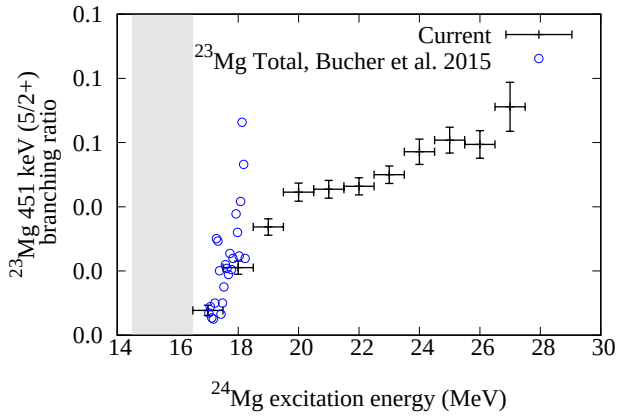

FIG. 13. (Color online) Neutron branching ratio populating the first excited state of ^{23}Mg. Higher excitation states were not measured, and γ cascading from these levels may be included at higher excitation energies. The total neutron branch found using the $^{12}C + {}^{12}C \rightarrow n + {}^{23}Mg$ cross section measurements of Bucher et al.[20] divided by the $^{12}C + {}^{12}C$ fusion cross section adopted by Caughlan and Fowler[21] is shown for comparison. This is not a direct comparison, since the current measurement does not include the branch to the ground state and only includes the portion of higher excited states which populate the first excited state in ^{23}Mg. The reference data thus serves as an upper limit for the current measurement.

this single γ-ray energy. The 4238 keV γ-ray offers one of the paths that bypasses the 1369 keV state. Other γ transitions which bypass both of these states are at energies greater than 5 MeV. The upper energy range for the γ-ray detectors was between 5 and 6 MeV depending on the specific detector and segment within the detector, thus the γ-decay channel for ^{24}Mg is mostly but not completely captured.

The final total branching ratios, shown in Fig. 15 have been normalized using the sum in Fig. 14 such that the sum of all branching ratios is 1. Since higher excited states of ^{20}Ne decay by α particle emission, these states are not included in the total for ^{20}Ne and are instead shown separately under the label ^{16}O, the resulting nucleus after ^{20}Ne emits an α particle. The total α branch is

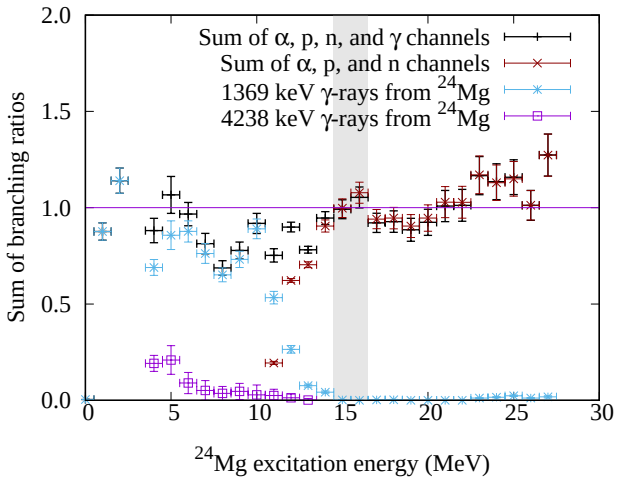

FIG. 14. (Color online) The sum of the measured γ, α, proton, and neutron channels. Note that in the energy range applicable to carbon burning (14 to 17 MeV) the sum is nearly one. The dip at 3 MeV is due to ^{24}Mg not having an excited state between 2.5 and 3.5 MeV. Additionally, many states in ^{24}Mg above 5 MeV have γ-decay branches which do not emit either a 1369 keV or a 4238 keV γ-ray, resulting in an underestimate of the total γ-decay branch between 5 MeV and the onset of the particle decay branches.

the sum of the branch leaving ^{20}Ne and the branch leaving ^{16}O as the product nucleus. This distinction only applies at higher excitation energies and not in the excitation energy range corresponding to the Gamow window for carbon burning.

V. CONCLUSION

Measurements of the branching ratios for the decay of ^{24}Mg excited by the inelastic scattering of 40 MeV α particles have been made. The range of excitation energies studied extends to 27 MeV. This range includes the excitation energies present in the ^{24}Mg compound nucleus formed in carbon burning reactions, which have excitation energies in the range of 15 to 16 MeV. This experiment was selected as a possible surrogate measurement for the branching ratios for the carbon burning compound nucleus, and consequently the ratios of the cross sections for the reactions $^{12}C + {}^{12}C \rightarrow {}^{20}Ne + \alpha$, $^{12}C + {}^{12}C \rightarrow {}^{23}Na + p$, and $^{12}C + {}^{12}C \rightarrow {}^{23}Mg + n$.

Comparisons of the measured branching ratios to those for $^{12}C + {}^{12}C$ show that at least for certain ranges of excitation energy that inelastic scattering of 40 MeV α particles produces a distribution of excited ^{24}Mg that favors decays into higher spin states of ^{20}Ne and ^{23}Na relative to the excited ^{24}Mg created as the compound nucleus in carbon burning. It suggests that the average spin distribution in the inelastically excited ^{24}Mg might be different from that of the ^{24}Mg compound nucleus in carbon burning.

While these differences prevent assigning a direct

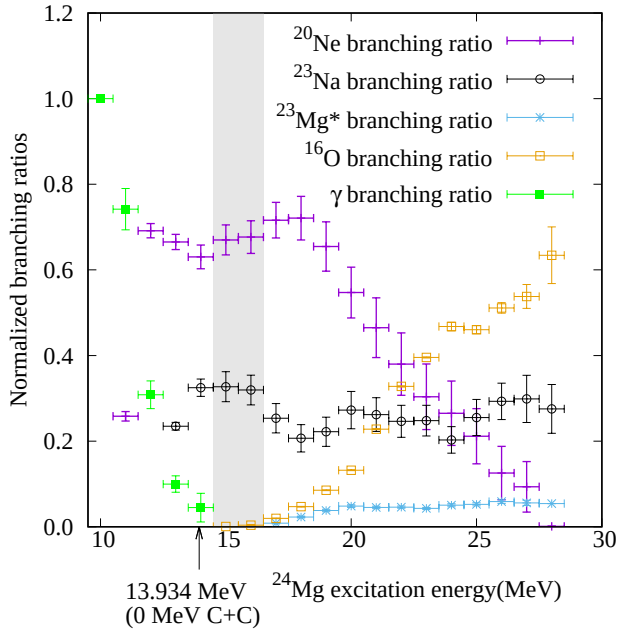

FIG. 15. (Color online) Total branching ratios for the α, proton, and neutron channels. The ratios are normalized by setting the total of all branches shown in Fig. 14 to one for all energies. No ground state contribution was assumed for the neutron channel. For equivalent $^{12}C + ^{12}C$ center of mass energies subtract 13.934 MeV from the ^{24}Mg excitation energy.

equality between the branching ratios found with inelastic scattering and in carbon burning, the branching ratios found in the inelastic scattering case do appear to have a relation to those in carbon burning which allow an estimate of the branching ratios for carbon burning to be made in the region of the Gamow window. The branching ratios to some states of ^{20}Ne and ^{23}Na were very similar for the inelastic scattering case and the carbon burning case. Additionally, as the excitation energy is decreased to the range of the Gamow window many of the branching ratios to the higher excited states diminish, reducing the total number of states which must be understood in order to predict the branching ratio.

It may be possible to approximately account for the different spin distributions by normalizing the surrogate results for each state to the direct $^{12}C + ^{12}C$ data, either individually or collectively as a function of the spin state. A formal justification for this correction would however require a more detailed understanding of the spin distribution in the direct and surrogate ^{24}Mg compound nuclei, therefore the results presented here do not include such a correction.

In the ^{24}Mg excitation energy range of 15 MeV to 16 MeV, the branching ratio to produce $^{20}\mathrm{Ne} + \alpha$ was measured to be $68 \pm 4\%$, and the branching ratio to produce $^{23}\mathrm{Na} + \mathrm{p}$ was measured to be $32 \pm 4\%$. If the effect of the probable angular momentum distribution difference between the $^{12}C + ^{12}C$ compound nucleus and ^{24}Mg excited by α scattering sufficiently diminishes at energies near the Gamow window, then these branching ratios are a good approximation of the branching ratios for the $^{12}C + ^{12}C$ reaction between 1 MeV and 2 MeV.

ACKNOWLEDGMENTS

This work was supported in part by the US Department of Energy under NNSA grants DE-FG52-09NA29467 and DE-NA0000979, Lawrence Livermore National Laboratory contract DE-AC52-07NA27344, Lawrence Berkeley National Laboratory contract DE-AC02-05CH11231, and Texas A&M Nuclear Physics grant DE-FG02-93ER40773.

[1] C. E. Rolfs and W. S. Rodney, *Cauldrons in the Cosmos* (The University of Chicago Press, Chicago 60637, 1988).
[2] J. M. Munson, *Decay Branching Ratios of Excited States in Mg24*, Ph.D. thesis, University of California-Berkeley (2015).
[3] N. Bohr, Nature **137**, 344 (1936).
[4] J. E. Escher, F. S. Dietrich, and C. Forssén, Nuclear Instruments and Methods in Physics Research Section B: Beam Interactions with Materials and Atoms **261**, 1075 (2007), the Application of Accelerators in Research and Industry - Proceedings of the Nineteenth International Conference on The Application of Accelerators in Research and Industry, Nineteenth International Conference on The Application of Accelerators in Research and Industry.
[5] J. E. Escher, J. T. Burke, F. S. Dietrich, N. D. Scielzo, I. J. Thompson, and W. Younes, Rev. Mod. Phys. **84**, 353 (2012).
[6] T. Spillane, F. Raiola, C. Rolfs, D. Schürmann, F. Strieder, S. Zeng, H.-W. Becker, C. Bordeanu, L. Gialanella, M. Romano, and J. Schweitzer, Physical Review Letters **98**, 122501 (2007).
[7] M. G. Mazarakis and W. E. Stephens, Physical Review C **7**, 1280 (1973).
[8] R. Dayras, Z. E. Switkowski, and S. E. Woosley, Nuclear Physics A **279**, 70 (1977).
[9] H. Becker, K. Kettner, C. Rolfs, and H. Trautvetter, Zeitschrift fr Physik A Atoms and Nuclei **303**, 305 (1981).
[10] L. Barrón-Palos, E. Chávez L., A. Huerta H., M. Ortiz, G. Murillo O., E. Aguilera R., E. Martnez Q., E. Moreno, R. Policroniades R., and A. Varela G., The European Physical Journal A - Hadrons and Nuclei **25**, 645 (2005), 10.1140/epjad/i2005-06-008-2.
[11] E. F. Aguilera, P. Rosales, E. Martinez-Quiroz, G. Murillo, M. Fernández, H. Berdejo, D. Lizcano, A. Gómez-Camacho, R. Policroniades, A. Varela, E. Moreno, E. Chávez, M. E. Ortíz, A. Huerta, T. Belyaeva, and M. Wiescher, Physical Review C **73**, 064601 (2006).
[12] L. Barrón-Palos, E. Aguilera, J. Aspiazu, A. Huerta,

E. Martínez-Quiroz, R. Monroy, E. Moreno, G. Murillo, M. Ortiz, R. Policroniades, A. Varela, and E. Chávez, Nuclear Physics A **779**, 318 (2006).
[13] S. Lesher, L. Phair, L. Bernstein, D. Bleuel, J. Burke, J. Church, P. Fallon, J. Gibelin, N. Scielzo, and M. Wiedeking, Nuclear Instruments and Methods in Physics Research Section A: Accelerators, Spectrometers, Detectors and Associated Equipment **621**, 286 (2010).
[14] F. S. Dietrich, "Simple derivation of the Hauser-Feshbach and Weisskoph-Ewing formulae, with application to surrogate reactions UCRL-TR-201718," (2004).
[15] J. E. Escher and F. S. Dietrich, Phys. Rev. C **81**, 024612 (2010).
[16] J. E. Escher and F. S. Dietrich, Phys. Rev. C **74**, 054601 (2006).
[17] V. F. Weisskopf and D. H. Ewing, Phys. Rev. **57**, 472 (1940).
[18] National Nuclear Data Center, "Q value calculator," `http://www.nndc.bnl.gov/qcalc/`, accessed: 2015-04-19.
[19] National Nuclear Data Center, `http://www.nndc.bnl.gov/`, accessed: 2015-06-15.
[20] B. Bucher, X. D. Tang, X. Fang, A. Heger, S. Almaraz-Calderon, A. Alongi, A. D. Ayangeakaa, M. Beard, A. Best, J. Browne, C. Cahillane, M. Couder, R. J. deBoer, A. Kontos, L. Lamm, Y. J. Li, A. Long, W. Lu, S. Lyons, M. Notani, D. Patel, N. Paul, M. Pignatari, A. Roberts, D. Robertson, K. Smith, E. Stech, R. Talwar, W. P. Tan, M. Wiescher, and S. E. Woosley, Phys. Rev. Lett. **114**, 251102 (2015).
[21] G. R. Caughlan and W. A. Fowler, Atomic Data and Nuclear Data Tables **40**, 283 (1988).